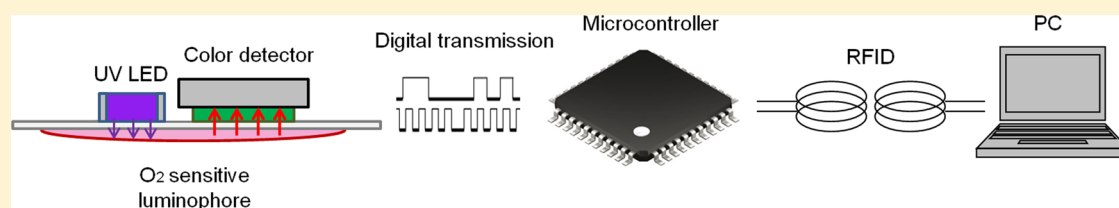


Screen Printed Flexible Radiofrequency Identification Tag for Oxygen Monitoring

A. Martínez-Olmos,^{*,†} J. Fernández-Salmerón,[†] N. Lopez-Ruiz,[†] A. Rivadeneyra Torres,[†]
L. F. Capitan-Vallvey,[‡] and A. J. Palma[†]

[†]ECsens, Department of Electronics and Computer Technology and [‡]Department of Analytical Chemistry, Campus Fuentenueva, Faculty of Sciences, University of Granada, E-18071 Granada, Spain



ABSTRACT: In this work, a radiofrequency identification (RFID) tag with an optical indicator for the measurement of gaseous oxygen is described. It consists of an O₂ sensing membrane of PtOEP together with a full electronic system for RFID communication, all printed on a flexible substrate. The membrane is excited by an LED at 385 nm wavelength and the intensity of the luminescence generated is registered by means of a digital color detector. The output data corresponding to the red coordinate of the RGB color space is directly related to the concentration of O₂, and it is sent to a microcontroller. The RFID tag is designed and implemented by screen printing on a flexible substrate for the wireless transmission of the measurement to a remote reader. It can operate in both active and passive mode, obtaining the power supply from the electromagnetic waves of the RFID reader or from a small battery, respectively. This system has been fully characterized and calibrated including temperature drifts, showing a high-resolution performance that allows measurement of very low values of oxygen content. Therefore this system is perfectly suitable for its use in modified atmosphere packaging where the oxygen concentration is reduced below 2%. As the reading of the O₂ concentration inside the envelope is carried out with an external RFID reader using wireless communication, there is no need for perforations for probes or wires, so the packaging remains completely closed. With the presented device, a limit of detection of 40 ppm and a resolution as low as 0.1 ppm of O₂ can be reached with a low power consumption of 3.55 mA.

The basis of the modern packaging technology surged in the 19th century with the invention of canning by Nicholas Appert and the later application of the food microbiology principles established by Louis Pasteur to the canning process.^{1,2} The main objective of packaging is the protection and preservation of food and beverage from external contamination. Food packaging can retard product deterioration, retain the beneficial effects of processing, extend shelf life, and maintain or increase the quality and safety of food. In this way, packaging protects from three major external influences: chemical, biological, and physical.³ Beyond this barrier function, there has been more research and development in the recent years regarding the introduction of new purposes to food packaging systems. Among these innovations, significant new functional packaging systems include smart and active packaging, modified atmosphere packaging (MAP), and edible films/coatings.⁴ Active packaging includes additives or components that can participate in a host of packaging applications and, by doing so, enhance the preservation function of the primary packaging system. Intelligent or smart packaging is packaging that somehow senses some properties of the food it encloses or the environment in which it is kept and is able to inform the manufacturer, retailer, and consumer of

the state of these characteristics.⁵ Intelligent packaging is an extension of the communication function of traditional packaging and communicates information to the consumer based on its ability to sense, detect, or record external or internal changes in the product's environment. Basically, there are two types of intelligent packaging: one based on measuring the condition outside the package, the other directly measuring the quality of the food product, i.e., inside the packaging. In the latter case, there is direct contact with the food or with its headspace and there is always the need for an indicative marker of the quality and/or safety of the packed food. Examples include time–temperature indicators (TTI), gas leakage indicators, ripeness indicators, toxin indicators, biosensors, and radio frequency identification.⁶

One of the most interesting parameter to be sensed in smart packaging is the concentration of oxygen within the package, since it is the main cause of food spoilage.⁷ The presence of oxygen facilitates processes such as promotion of microbial growth, lipid oxidation, protein decomposition, and discolor-

Received: September 10, 2013

Accepted: October 14, 2013

Published: October 14, 2013

ation.⁸ Therefore, it is common to seal the food in an ambient atmosphere that is low in oxygen, usually in the 0.5–2% range⁹ or even less.¹⁰ Different types of oxygen sensors and indicators for MAP have been reported in the literature, being the most popular visual indicators.^{11–13} In this kind of indicators, a color change is observed, in most cases, due to either an oxygen-binding reaction, a redox reaction, or a light-activated redox reaction.^{12,14} Apart from these colorimetric indicators, luminescence-based sensors offer an alternative to a purely visual response.^{15–17} This optical technique can be used for the quantitative measurement of the O₂ concentration in a nondestructive manner and has the advantage of addressing misreading due to the sensitivity limitations of human eyesight. Nevertheless, additional electronics is required, thus, increasing the cost of the system.

Intelligent packaging is often combined to radio frequency identification (RFID) tags. This technology uses tags affixed to assets (cattle, containers, pallets, etc.) to transmit accurate, real-time information to a user's information system. RFID technology has been available for approximately 40 years although its broad application to packaging is a relatively recent development.⁵ In the literature, applications of RFID to the control of perishable foods¹⁸ and multigas detection have been reported.^{19,20}

In previous work, the authors presented portable instrumentation for the determination of gaseous oxygen based on the quenching of the well-known O₂ luminophore platinum octaethylporphyrin (PtOEP).^{21,22} The use of photodiodes coated with a stabilized polystyrene membrane containing PtOEP makes it possible to sense O₂ using an analytical parameter similar to lifetime^{23,24} and also the intensity of the luminescence in a stationary excitation state which is quantified by a color measurement.²⁵

Here, this luminophore is used to create a tag for smart packaging oriented to the monitoring of oxygen in a modified atmosphere. An O₂ sensitive membrane of PtOEP is printed in the inner surface of a flexible polymeric substrate, polyethylene naphthalate (PEN), which acts as the package envelope. The measurement system is printed on the outer surface. It consists of the excitation and reading electronics compounded with a light-emitting diode (LED), a color detector, and a radio frequency identification (RFID) tag which allows a wireless transmission of the measurement. This is a high-resolution, long-life system for the determination of the oxygen concentration which allows users (producer, distributor, seller, or consumer) to monitor the content of O₂ inside the package with a simple RFID reader using a standard communication protocol.

■ EXPERIMENTAL SECTION

Reagents and Materials. The chemicals used were as follows: platinum octaethylporphyrin complex (PtOEP, Porphyrin Products Inc., Logan, UT), 1,4-diazabicyclo[2.2.2]octane (DABCO, 98%), tetrahydrofuran (THF) and polystyrene (PS, average MW 280 000; T_g, 100 °C; GPC grade). All three supplied by Sigma–Aldrich Química S.A. (Madrid, Spain). The gases O₂ and N₂ (>99%) were supplied in gas cylinders by Air Liquide S.A. (Madrid, Spain).

A 120 Nylon threads per centimeter (T/cm) mesh were used to manufacture the screen printed patterns. The tags were printed with SunTronic CRSN 2442 silver ink (Sun Chemical, Parsippany, NJ) and consisted of one printed layer with a Serfix

III screen printing machine (Seglevint SL, Barcelona, Spain). Finally the curing process took place at 120 °C for 5 min.

The chosen substrate was 125 μm thick polyethylene naphthalate (PEN, Kaladex PEN Film, Dupont Teijin Films, Japan). The film must present a high transparency to visible light due to application requirements. Polyethylene terephthalate (PET) is widely used in packaging applications, so it was considered in the first place. PEN polyester is chemically quite similar to PET but is more temperature resistant and certified for long-term electrical use. Although both materials have a high optical transmission (>85%) in the visible spectrum, PEN was finally selected because of its better adherence. It is, however, more expensive and has worse bending properties.

A two-step process was developed to do the transfer of chips. First a conductive-adhesive resin, H20E (Epoxy Technology Inc., Billerica, MA), was used to make the interconnections between integrated circuits and printed silver pad. A double layer 50 μm-thick dry adhesive, AR Clear 8932 (Adhesives Research, Inc. Glen Rock, PA), was placed on the bottom part of the chips to fix them to the substrate. The last step was heating up in an oven at 120 °C for 20 min to cure the conductive resin. Furthermore, the dry film adhesion improved with temperature, so the heat treatment served also to better fix the chips to the substrate.

Instruments and Software. For the electrical characterization of the system, the following instrumentation was used: a mixed signal oscilloscope (MSO4101, Tektronix, Beaverton, OR), an 81/2-bit Digital Multimeter 3158A (Agilent Technologies, Santa Clara, CA), a 15 MHz waveform generator 33120A (Agilent Technologies, Santa Clara, CA), an E5071C network analyzer, a N4431A kit (Agilent Technologies, Santa Clara, CA), a Precision Impedance Analyzer 4294A and an impedance probe kit (4294A1) (Agilent Technologies, Santa Clara, CA), a dc power supply E3630A (Agilent Technologies, Santa Clara, CA) and a RFID reader TRF7960 (Texas Instruments, Dallas, TX), and a balance DV215CD (Ohaus Co., Pine Brook, NJ). A user interface made in Visual Basic was used in a computer for calibration purposes. The standard mixtures for instrument calibration and characterization were prepared using N₂ as the inert gas by controlling the flow rates of the different high purity gases O₂ and N₂, entering a mixing chamber using a computer-controlled mass flow controller (Air Liquid España S.A., Madrid, Spain) operating at a total pressure of 760 Torr and a flow rate of 500 cm³ min⁻¹.

A thermostatic chamber, with a lateral hole for the connection to a computer and gas tubing entrance, made it possible to maintain a controlled temperature between –50 °C and +50 °C with an accuracy of ±0.1 °C for thermal characterization of the tag.

Advanced Design Simulator (ADS, Agilent Technologies, Santa Clara, CA), a software based on the momentum method, was for simulating the electrical behavior of the printed antennas, including the surface roughness and the substrate influence on the rf performance.

Membrane Preparation. The cocktail for the preparation of the oxygen-sensitive membrane were made by dissolving 0.5 mg of PtOEP and 12 mg of DABCO in 1 mL of a solution of 5% (w/v) of PS in freshly distilled THF. The sensitive membrane was cast by placing a volume of 10 μL of the cocktail on a flexible substrate using the spin-coating technique under ambient atmospheric conditions. After the deposition of the sensing membranes, the substrate containing them was left to dry in darkness in a THF atmosphere for 1 h. The obtained

membranes were homogeneous, transparent, and pink colored. The sensing membranes containing PtOEP in PS are recommended to be cured in darkness for 9 days before their use.²⁶ When they are not in use, they must be kept in darkness to extend their lifetime.

Description of the System. The monitoring system for intelligent packaging presented here determines the concentration of gaseous O₂ by means of the measurement of the intensity of the luminescent emission generated in the membrane which is quenched by O₂. Classically, the scheme for the intensity measurement consists of a photodetector such as a photodiode that generates a current proportional to the incident light. Nevertheless, it is possible to substitute this kind of photodetectors by color detectors, whose output is a signal proportional to the color of the incident light and the intensity of this color.²⁷ This strategy for the quantification of light intensity has proven to be highly sensitive and allows discarding external interferences.^{25,28,29} Therefore, here it is used instead of the classical light measurement through photodiodes.

The emission spectrum of the oxygen sensitive membrane presents a peak at a wavelength of 645 nm. That means that this luminophore generates a red luminescence when it is optically excited. Thus, a measurement of the intensity of a luminescence can be carried out by the color detector, since the reading of the red (R) coordinate includes this intensity measurement. For this reason, the color data obtained from the digital detector are processed here in the RGB color space rather than other spaces. In addition, the color detector used in this work provides the color reading directly in this space as R, G, and B components, avoiding further processing and transformation between color spaces.

The system can be considered to be formed by two blocks: the sensing module, which excites the oxygen sensitive membrane and detects the luminescence, and the transmitting module formed by a RFID tag for the remote reading of the measurement.

Sensing Module. The sensing module is schematized in Figure 1. This block is formed by the excitation and detection electronics together with the oxygen sensing membrane.

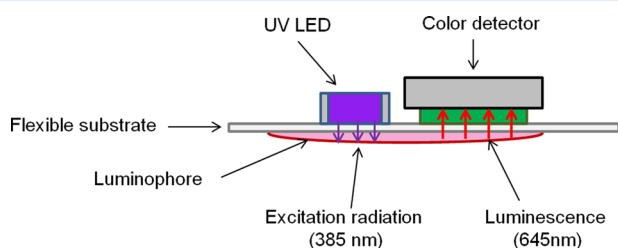


Figure 1. Side view of the sensing module.

The optical excitation of the membrane is carried out using a surface-mount LED (OCU-400UE390, OSA Opto Light, Berlin, Germany) with peak emission at 385 nm. The luminescence generated by the luminophore when it is optically excited is dynamically quenched by oxygen, thus causing changes both in phosphorescence intensity and lifetime.^{30–32} In this case, luminescence intensity is selected to be related to the concentration of the surrounding gaseous oxygen. This emission is registered by means of a color detector model S9706 (Hamamatsu Photonics, Japan). This device is a digital color sensor sensitive to red ($\lambda_p = 615$ nm, the wavelength of maximal sensitivity), green ($\lambda_p = 540$ nm), and blue ($\lambda_p = 465$

nm) spectral regions, which makes possible the simultaneous measurement of RGB color coordinates. The detected light is coded by the digital detector into 36-bit words, which make it possible to connect directly the sensors to the microcontroller. To enable measurement over a wide range of illuminants, the S9706 detector has two configuration parameters to select its active area and integration time. Internally, the active area of each detector (with dimensions of 1.2 mm \times 1.2 mm) consists of 9 \times 9 silicon photodiode elements in a mosaic, alternating red, blue, and green sensitivity, and it can be configured in a high sensitivity mode, where the full area collects the incident light, or in a low sensitivity mode, where a 3 \times 3 center area is chosen to be active. In this work, a high sensitivity mode was always chosen to cover a wide membrane surface. The integration time can be modified by software, and it determines the temporal window in which the detector is collecting the incident light. The response time and resolution of the system are depending on this parameter, as it will be explained below.

Although simultaneous reading of the RGB components in the incident light is provided, only the red and blue coordinates are considered in this case, with the green value irrelevant. When the system is optically isolated to avoid external light interference, the R value corresponds exclusively to the luminescence generated by the PtOEP complex and its value depends on the intensity of this emission and, therefore, on the O₂ concentration.^{25,29} The B value of the reading is related to the visible emission of the LED, and it is used as a reference signal to correct fluctuations in the source illumination.³³

As it can be seen in Figure 1, the layout of these components is as follows: the luminophore is deposited on the inner surface of flexible substrate (PEN). In this way, this is the only element of the system that is placed inside the package, whereas the full electronics is printed on the outer side of the substrate. The LED for the optical excitation as well as the color detector are placed very close to one another and directly facing the membrane from the external side of the substrate. Although in the literature similar dispositions of the sensing elements are reported, it is common to manipulate the substrate in an effort to make a waveguide to transport the excitation and response emissions.^{34–36} It inevitably implies optical losses in the propagation of the light.³⁵ In order to avoid these losses, in this work the package surface is treated merely as a substrate for the system, and both the exciting emission as the response luminescence travel directly from the LED to the membrane and from the membrane to the color detector, as depicted in Figure 1.

Both the LED and the S9706 detector are connected directly to a microcontroller model PIC18F46J50 (Microchip Technology Inc., Chandler, AZ) which has been selected because of its low power consumption (nanoWatt XLP Technology). In order to avoid thermal drifts, the LED is biased in a pulsed mode by the microcontroller, which introduces a pulse train of a high frequency (500 kHz) and 3.3 V between its terminals. This biasing configuration eliminates the use of a current source in the design, thus simplifying the system, as it will be explained below.

RFID Module. The block diagram of the proposed RFID tag is presented in Figure 2. It is a microcontroller-based system designed for a wireless transmission of the oxygen concentration within the package.

This scheme is aimed to transmit the measured data using the protocol ISO15693 which operates in the high frequency (HF) band (13.56 MHz) and has a maximum reading distance

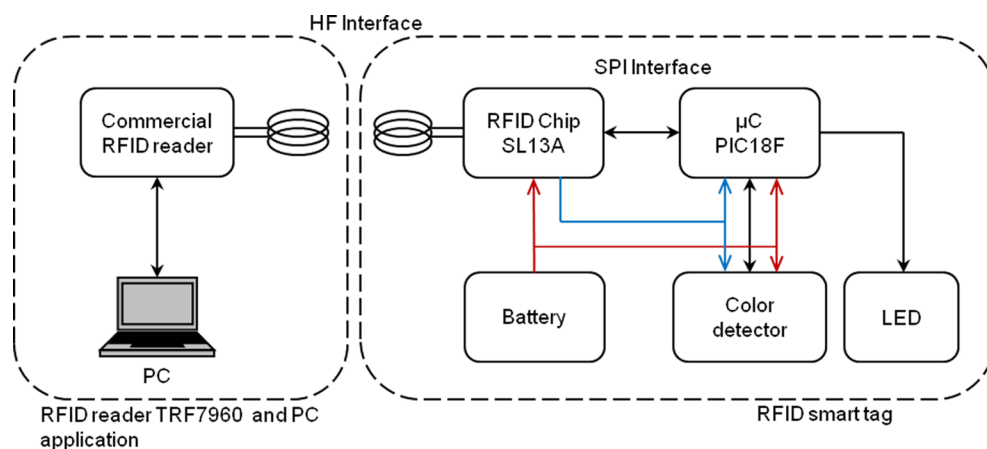


Figure 2. Block diagram of the developed RFID tag. Black connections represent data lines, red connections are principal power lines, and blue connections are secondary power lines.

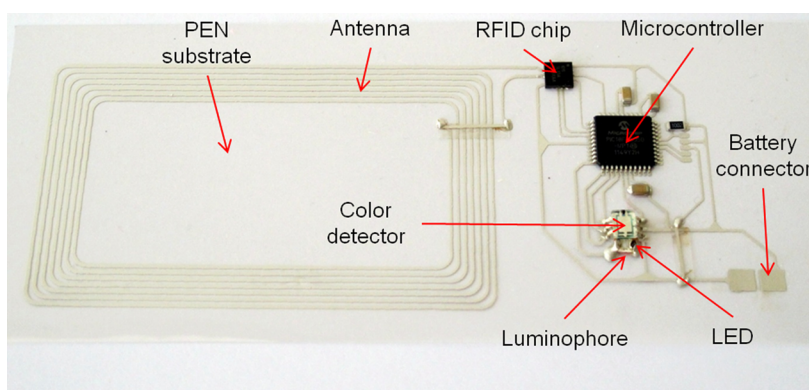


Figure 3. Photograph of the system: the sensing module has been uncovered to show its structure.

about 1–1.5 m for active RFID tags.³⁷ The objective is to print the designed antenna and all the electronics on a flexible substrate which makes the package.

The SL13A (IDS Microchip AG, Wollerau, Switzerland) has been selected as the RFID chip. This device includes, apart from the rf interface, an on-chip 8k bit EEPROM and an on-chip temperature sensor. In rf mode, using the ISO15693 protocol, the RFID chip is accessed via a 13.56 MHz electromagnetic carrier wave on which incoming data are demodulated from the received amplitude modulated signal. Apart from the rf interface, this chip works with the SPI interface, which allows access to its EEPROM memory and temperature data through the microcontroller. In this regard, it is possible to store data on the RFID chip memory that could be read out easily by a commercial RFID reader. In addition, the IDS-SL13A is supplied from either the battery or through the rf field from a reader, making it possible to operate in passive or active mode. The chip has an internal regulator capable of providing a voltage output of 3.4 V and a maximum current of 4 mA for the rest of the circuitry when it is supplied from the reader. Therefore, it is possible to configure the system as a passive tag that only measures the oxygen when the user requires a reading, with no need of additional power supplying (blue powering lines in Figure 2). Nevertheless, in this work a battery is included to give the option of a periodic oxygen measurement and data storing when the external RFID reader is not present (red lines in Figure 2). In this second operation mode, the measured values of oxygen and temper-

ature including a timestamp in UTC format are stored on the system memory. Furthermore, the system can be configured to store the information only when the acquired data is out of threshold values by setting the highest and lowest values of oxygen detection.

The antenna is a custom-designed screen printed inductor. This kind of coils has been reported in the recent literature,^{38,39} and it has been selected here due to its flexibility which makes it proper to be implemented on an intelligent package. The RFID chip has a capacitance of about 25 pF at the frequency of interest. Resonance occurs when $\omega_0 = 1/\sqrt{LC}$, thus a value of 5.5 μH for the coil antenna must be achieved to resonate at the desired frequency without including external capacitances. The start point to design and optimize the HF coil antennas has been extracted from the Wheeler model which presents simple expressions for planar inductance calculation.⁴⁰ Next, ADS software has been used to simulate the inductors in order to find the appropriate dimensions for the specific inductance at 13.56 MHz, using the simulator capabilities to optimize the final design through the maximization of the quality factor keeping the desired value of inductance on reasonable interval values. Using the 120 (T/cm) screen printing mesh on the PEN substrate, the obtained resistivity for SunTronic CRSN 2442 paste ink is around 40 $\mu\Omega\text{ cm}$, whereas the obtained thickness is 13.37 μm .⁴¹ All these parameters have been taken into account in simulation. The printed coil inductor is finally designed with seven turns and dimensions of 75 mm \times 45 mm.

The width of the conductor and the interspacing between the lines are each 600 μm .

A polymer lithium-ion battery PGEB01 (General Electronics Co, Shenzhen, P.R. China) has been used to power on the tag when it is used in active mode. This is a rechargeable battery of 3.7 V and a charge of 40 mAh. A HF band commercial reader, TRF7690EVM (Texas Instrument Inc.) fully compatible with ISO15693 protocol, has been used to test the developed RFID tag. A Visual Basic application (Microsoft Corp., Redmond, WA) has been developed to configure and read out the manufactured RFID tag.

RESULTS AND DISCUSSION

Figure 3 presents a photography of the full system, where all the components described in the previous section are marked. It is to be noted that the sensing block must be darkened in order to avoid external light interference. This can be done by covering the sensing module with adhesive black insulating tape or attaching a black coating layer on the inner surface of the substrate, leaving a small aperture where the LED and the color detector are placed.

As explained above, the luminophore is excited with a radiation of 385 nm generated using an UV LED. This corresponds to one of the absorption peaks of the PtOEP complex, with the other at 537 nm wavelength which has been used in other works.^{32,42} Nevertheless, in those previous cases the measurement of the gaseous oxygen was based on the lifetime of the luminescence generated in the sensing membrane. In this work, a relationship between the oxygen concentration and luminescence intensity is searched, and this intensity is quantified by means of a digital color detector. For that reason, an excitation in the UV range is selected in order to avoid environmental light interferences in the light detection.²⁵

System Calibration. The detection of the light intensity is carried out after the membrane is excited by the UV radiation emitted by the LED. In previous work, this LED was biased using a custom-designed current source that lead the LED to a steady state in which it drove a fixed current. In this state, the precise moment to take the measurement became critical, since the excitation with the UV radiation produces an increase in the temperature over time that affects the intensity of the emitted luminescence.²⁵ To overcome this situation, in this work the LED is directly biased through the microcontroller, which introduces a voltage pulse train between the terminals of the LED of 3.3 V high and 500 kHz. In consequence, the current source is not necessary and the number of components in the electronics and, thus, the consumption of the systems are reduced. The high frequency in the biasing of the LED implies a period of alternating between on and off states for the LED of 2 μs , much lower than the response time of the luminophore which is in the range of hundreds of microseconds.⁴² Therefore, the sensing membrane is not affected by this LED commutation, and thermal drifts are minimized. In addition, the integration time of the color detector S9706 varies in the range of hundreds of milliseconds, as will be explained below; in this period of time the detector is collecting incident light, and variations of the luminescence due to the LED commutation are minimized by the integration of the total incident light in this period. In this situation, the light measurement can be carried out at any moment after the LED is polarized. However, a small delay of 0.5 s is elapsed before the measurement in order to get a stabilized state of the LED. Moreover, fluctuations of the emitted radiation of the

LED can appear if the power line of the microcontroller is not completely stable. These fluctuations can introduce variations in the membrane response with deeper effects than those due to the LED commutation. In order to correct this effect, the R coordinate given by the color detector is normalized by the B coordinate, whose value corresponds to the LED radiation captured by the color detector. Consequently, the oxygen concentration is related to the ratio R/B, being R and B the values of the red and blue coordinates given by the color detector S9706.³³

The relationship between oxygen concentration and the value of the R/B coefficient is shown in Figure 4a, where the

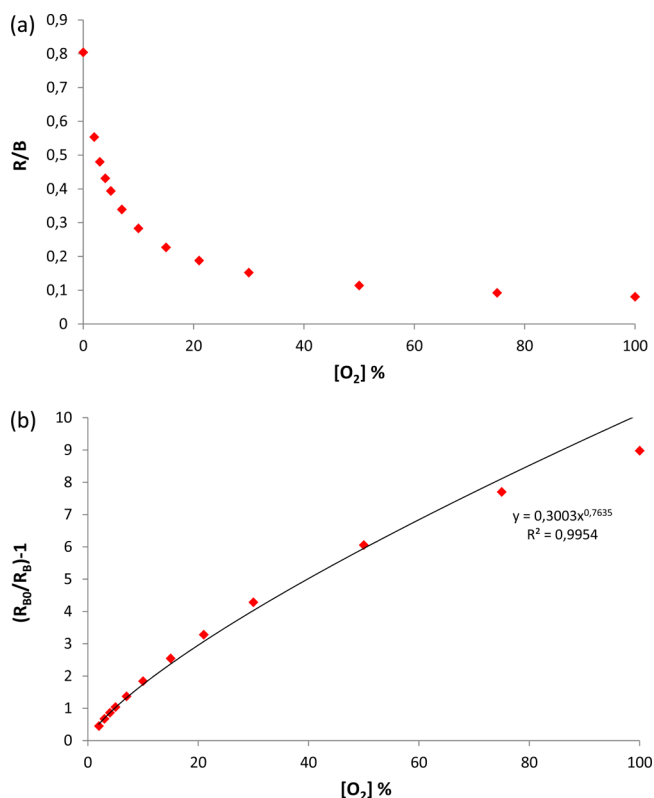


Figure 4. (a) Response curve and (b) calibration curve of the oxygen RFID tag (21 °C). Average error is 6×10^{-4} (a) and 3×10^{-3} (b).

response curve of the system in the full range 0–100% O_2 is presented. These data include six replicas at room temperature (21 °C) and the integration time of the color detector was set to 200 ms. Although error bars are included in this figure (and following ones), they are too small to be appreciated.

As it can be seen, the intensity of the luminescence decreases with the oxygen concentration. The response curve in Figure 4a can be fitted to a Freundlich isotherm for luminescence which models a nonlinear Stern–Volmer behavior and can be represented in the simplest form as⁴³

$$\left(\frac{I_0}{I}\right) - 1 = \alpha[\text{O}_2]^\beta \quad (1)$$

where I is the intensity of the emitted luminescence, I_0 the intensity in the absence of oxygen, and α and β are fitting parameters. The fitting curve for the response of the sensor is presented in Figure 4b, for which $\alpha = 0.30$ and $\beta = 0.7635$ (correlation factor $r^2 = 0.995$).

The parameters R_B and R_{B0} denote the ratios R/B and R_0/B_0 , respectively, which correspond to the measurement of the intensity of the luminescence in the presence and absence of oxygen, as explained above.

The technical specifications of the system, such as resolution and response time, depend directly on the integration time selected for the measurement. This parameter establishes the period of time in which the color detector is collecting the incident light. It is evident that the output data of the detector is higher if this time is longer, resulting in better characteristics of the system. In Figure 5, several response curves of the

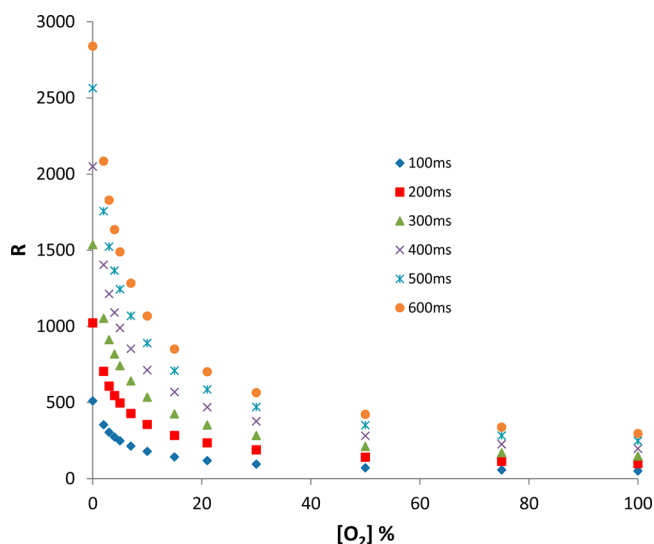


Figure 5. Response curves for different integration times.

sensitive membrane, corresponding to different integration times, are depicted. As it can be seen, the higher the integration time, the broader the range of the R coordinate, which implies a better resolution, as it will be exposed in the following figure.

The theoretical resolution of this system can be derived from the fitting curve of eq 1 by taking derivatives in both sides, approximating these derivatives to increments and reorganizing the terms, so that the theoretical resolution is obtained as

$$\Delta O_2 = \frac{I_0 \left(\frac{I_0 - I}{I - \alpha} \right)^{1/\beta} \Delta I}{I \cdot \beta (I - I_0)} \quad (2)$$

where ΔI is the error in the determination of the coefficient R/B , which is given by

$$\Delta I = \frac{1}{R} \Delta R + \frac{R}{B^2} \Delta B \quad (3)$$

being $\Delta R = \Delta B$ the maximum resolution in the measurement of the light. This parameter is related to the resolution of the color detector. Although it is not specified in the datasheet of the S9706, it is common to take a reading error of ± 4 LSB (least significant bit) for the internal analog to digital converter in these devices. Therefore, taking into account that the resolution of the color detector is 12 bits, the value for ΔR and ΔB is 0.19%. From eqs 2 and 3, the results of resolution for the different integration times in Figure 5 are calculated at several oxygen concentrations and presented in Table 1. These data confirm that better values of the resolution are achieved when higher integration times are used, being the maximum reachable without producing a saturation of the detector of

Table 1. Theoretical Resolution of the System in ppm at Different O_2 Concentrations at Room Temperature (21 °C)

integration time (ms)	2% O_2	10% O_2	21% O_2
100	0.6	3.0	7.7
200	0.3	1.5	3.8
300	0.2	1.0	2.6
400	0.2	0.8	1.9
500	0.1	0.6	1.5
600	0.1	0.5	1.3

0.1 ppm of O_2 . This value significantly improves the resolution obtained in previous works,^{23,42} where the resolution was 5000 and 500 ppm, respectively. These results demonstrate that quantifying the intensity of the luminescence by a high-resolution color detector is a good alternative to classical measuring approaches where the intensity of the signal is registered by simple photodetectors. The accuracy achieved with the RFID tag depends on the oxygen concentration, being 0.01% and 0.08%, as the standard deviation ($n = 5$) at 2% and 21% of O_2 , respectively.

Another important technical parameter is the limit of detection (LOD). This parameter was obtained using the standard criteria: $LOD = y_b + 3s_b$, where y_b is the average blank signal and s_b is the standard deviation of the blank, which is determined using at least 10 replicates. In this case, the LOD is independent of the integration time and takes a value of 40 ppm of O_2 , which confirms that the system here presented is suitable for smart packaging where the food are preserved at very low oxygen concentrations.

Temperature Dependence. As discussed in previous work, the temperature has a notable influence on the quenching produced by the oxygen in the light emission of a luminophore.^{25,42} Therefore, this effect has to be characterized and corrected. With this aim, a study of the instrument response for different temperatures was carried out. Figure 6

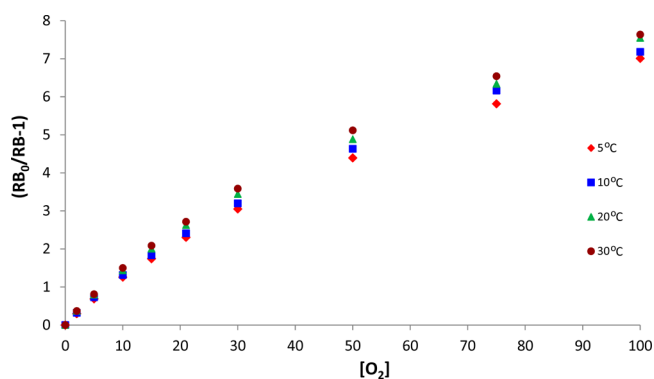


Figure 6. Thermal dependence of the oxygen RFID tag.

represents the instrument response at different temperatures. The curves were obtained using six replicates for each oxygen concentration at a given temperature. As it can be seen, the increase in the temperature reduces the intensity of the luminescence generated by the membrane causing a lower red signal. This effect was modeled introducing the thermal dependence in the fitting parameters α and β which can be expressed as a polynomial function of the temperature in the form $\alpha = -1.09 \times 10^{-5} T^3 + 5.14 \times 10^{-4} T^2 - 4.35 \times 10^{-3} T + 0.198$ ($r^2 = 0.981$), $\beta = 8.22 \times 10^{-6} T^3 - 3.85 \times 10^{-4} T^2 + 3.39 \times 10^{-3} T + 0.797$ ($r^2 = 0.987$) with T in degrees Celsius.

As it has been exposed above, the RFID chip used in this work has an on-chip temperature sensor which is able to obtain temperature readings in the range -40 to 60 °C with an accuracy of 0.5 °C. The 10 bits temperature value is obtained from the RFID chip through an on-chip A/D converter which uses a calibrated bandgap reference as a reference voltage. Through this feature, it is possible to correct the measurement of the oxygen including the previous modeling of the fitting parameters α and β in the microcontroller.

Antenna Tag Characterization. The antenna characterization has been carried out by means of both simulation and experimental analysis. The rf electrical characterization of the fabricated coil inductors has been performed by measuring their inductance quality factor and equivalent circuits. The measurements have been done using the four-point measurement technique. Results confirm that the inductance value of the coil is hardly affected by the substrate.⁴¹ The values obtained by simulation for the induction and quality factor are 5.62 μH and 2.676 , respectively, whereas the experimental values are 5.8 μH and 3.5 at the resonance frequency of 13.56 MHz. Although these values are in agreement, the mismatch could be explained by the reduction of the self-resonant frequency of the inductors, 32 MHz, was slightly lower than the simulated one, 35 MHz, as shown in Figure 7a.

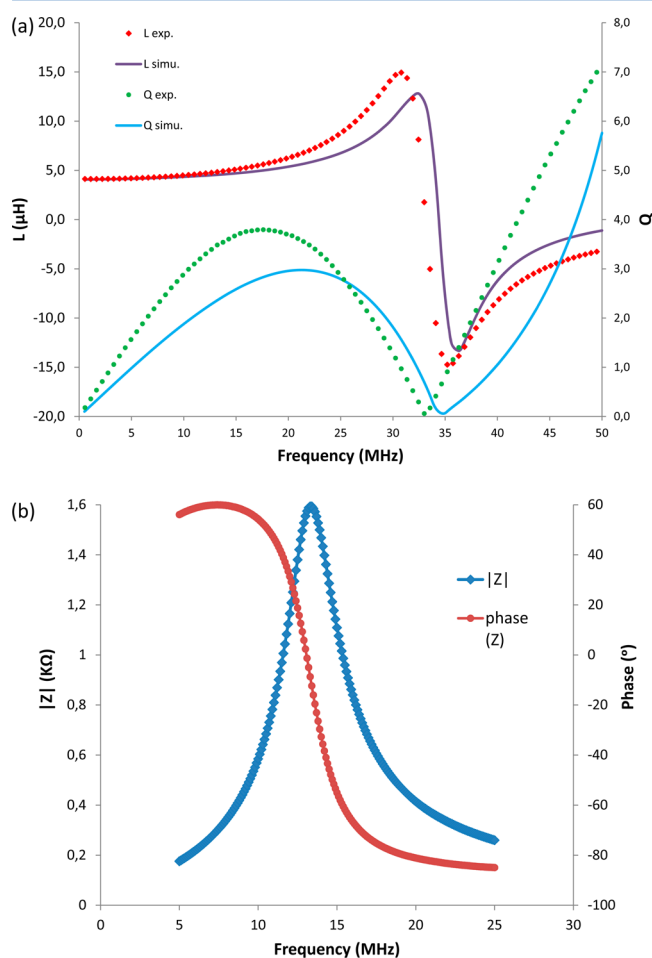


Figure 7. (a) Simulated (lines) and measured (symbols) frequency response of the antenna; (b) impedance of the tag as a function of the frequency.

The operation of the antenna tag has been tested with the commercial RFID reader TRF7960 with a read range of around 12 cm in vertical direction and 11.2 cm in horizontal one in passive operation mode. The resonance frequency of the full system antenna-RFID chip has been evaluated through an impedance analyzer. In Figure 7b, the impedance of the tag is presented, where it has been decomposed in phase and module. As it can be observed, the impedance reaches a value of 1.6 k Ω at the resonance frequency, that is the one at which the phase is null, in this case 13.6 MHz. Although this value is not exactly the working frequency searched of 13.56 MHz, it is perfectly valid for a wireless operation following the ISO15693 protocol specification related to the anticollision mechanism that establishes a tolerance range of ± 7 kHz around this center frequency.

The proper operation of the label has been tested satisfactorily through the developed Visual Basic application. Battery power is not necessary to access the stored data on the RFID chip making the label a semipassive smart tag for sensing applications. The power consumption of the RFID tag is only 34.4 μA in idle mode and 3.55 mA in sensing mode. This value is low enough (below 4 mA) to be provided by the internal regulator of the SL13A RFID chip, which makes it possible to operate as a passive tag with no need for an extra battery.

CONCLUSIONS

In this work, a novel design for the monitoring of gaseous oxygen that could be used in the interior of modified atmosphere packaging is presented. It consists of a smart packaging on whose inner surface an oxygen sensitive membrane is disposed, whereas the needed electronics is printed on the outer side of the package surface. For testing purpose, the system has been implemented on a piece of PEN flexible substrate by means of a screen printing technique where silver ink is used to trace the tracks between components. In this design, a RFID tag for the data transmission is also included. This tag can operate either in active or passive mode, obtaining the power supply from a battery or the electromagnetic field of an external RFID reader, respectively. The reading of the oxygen concentration inside the envelope can be carried out with an external RFID reader using a wireless communication. This means that the packaging remains completely closed, with no need of perforations for probes or wires. A full characterization of the antenna has been carried out by means of simulations and experimental analysis, showing a good agreement in the results and proving that flexible RFID tags are recommended for this application.

The measuring electronics are based on a 12-bit digital color detector which measures the intensity of the emitted luminescence, quenched by the surrounding gaseous oxygen. Thanks to its high-resolution, readings of O_2 can be realized at concentrations as low as 40 ppm with very low error levels in the order of 0.1 ppm of O_2 . Temperature drift is corrected through the on-chip temperature sensor. Therefore, this system is highly suitable for its application in the measurement of oxygen concentration in modified atmosphere packaging with a reduced oxygen concentration.

AUTHOR INFORMATION

Corresponding Author

*E-mail: amartinez@ugr.es.

Notes

The authors declare no competing financial interest.

ACKNOWLEDGMENTS

This work was partially funded by the Junta de Andalucía (Proyecto de Excelencia P10-TIC-5997 and P10-FQM-5974). These projects were partially supported by European Regional Development Funds (ERDF). We also acknowledge financial support from Project PYR-2012-12, CEI BioTIC (CEB09-0010 and CEI2013-P-2) from CEI program of MICINN.

REFERENCES

- (1) Brody, A. L.; Bugusu, B.; Han, J. H.; Sand, C. K.; Mchugh, T. H. *J. Food Sci.* **2008**, *733*, R107–R116.
- (2) Wilson, C. *Frontiers of Intelligent and Active Packaging for Fruits and Vegetables*; CRC Press: Boca Raton, FL, 2007.
- (3) Marsh, K.; Bugusu, B. *J. Food Sci.* **2007**, *72*, R39–R55.
- (4) Han, J. H. *Innovations in Food Packaging*; Academic Press: San Diego, CA, 2005.
- (5) Kerry, J. P.; O'Grady, M. N.; Hogan, S. A. *Meat Sci.* **2006**, *74*, 113–130.
- (6) Restuccia, D.; Spizzirri, U. G.; Parisi, O. I.; Cirillo, G.; Curcio, M.; Iemma, F.; Puoci, F.; Vinci, G.; Picci, N. *Food Control* **2010**, *21*, 1425–1435.
- (7) Rooney, M. L. *Active Food Packaging*; Blackie Academic & Professional: London, 1995.
- (8) Mills, A.; Lawrie, K.; Bardin, J.; Apedaile, A.; Skinner, G. A.; O'Rourke, C. *Analyst* **2012**, *137*, 106–112.
- (9) Blakistone, B. A., Ed. *Principles and Applications of Modified Atmosphere Packaging of Foods*, 2nd ed.; Blackie Academic & Professional: London, 1998.
- (10) Faustman, C.; Cassens, R. G. *J. Muscle Foods* **1990**, *1*, 217–243.
- (11) Smolander, M.; Hurme, E.; Ahvenainen, R. *Trends Food Sci.* **1997**, *8*, 101–105.
- (12) Mills, A. *Chem. Soc. Rev.* **2005**, *34*, 1003–1011.
- (13) Evans, R. C.; Douglas, P.; Williams, J. A.; Rochester, D. L. *J. Fluoresc.* **2006**, *16*, 201–206.
- (14) Mills, A.; Hazafy, D. *Analyst* **2008**, *133*, 213–218.
- (15) Reininger, F.; Kolle, C.; Trettnak, W.; Gruber, W. Quality Control of Gas-packed Food by an Optical Oxygen Sensor. *Proceedings of the International Symposium on Food Packaging: Ensuring the Safety and Quality of Foods*, Budapest, Hungary, September 11–13, 1996.
- (16) O'Riordan, T. C.; Voraberger, H.; Kerry, J. P.; Papkovsky, D. B. *Anal. Chim. Acta* **2005**, *530*, 135–141.
- (17) Papkovsky, D. B.; Papkovskaia, N.; Smyth, A.; Kerry, J.; Ogurtsov, V. *Anal. Lett.* **2000**, *33*, 1775–1777.
- (18) Atsushi, O.; Kentaro, Y. *NEC Tech. J.* **2006**, *1*, 82–86.
- (19) Steinberg, I. M.; Steinberg, M. D. *Sens. Actuators, B: Chem.* **2009**, *138*, 120–125.
- (20) Eom, K. H.; Kim, M. C.; Lee, S. J.; Lee, C. W. *Int. J. Distrib. Sens. Network* **2012**, *2012*, 1–6.
- (21) Quaranta, M.; Borisov, S. M.; Klimant, I. *Bioanal. Rev.* **2012**, *4*, 115–157.
- (22) Demas, J. N.; DeGraff, B. A. *Coord. Chem. Rev.* **2001**, *211*, 317–351.
- (23) Palma, A. J.; López-González, J.; Asensio, L. J.; Fernandez-Ramos, M. D.; Capitán-Vallvey, L. F. *Sens. Actuators, B: Chem.* **2007**, *121*, 629–638.
- (24) Martínez-Olmos, A.; Pérez de Vargas-Sansalvador, I. M.; Palma, A. J.; Banqueri, J.; Fernández-Ramos, M. D.; Capitán-Vallvey, L. F. *Sens. Actuators, B: Chem.* **2011**, *160*, 52–58.
- (25) López-Ruiz, N.; Martínez-Olmos, A.; Pérez de Vargas-Sansalvador, I. M.; Fernández-Ramos, M. D.; Carvajal, M. A.; Capitán-Vallvey, L. F.; Palma, A. J. *Sens. Actuators, B: Chem.* **2012**, *171*, 938–945.
- (26) Pérez de Vargas-Sansalvador, I. M.; Carvajal, M. A.; Roldan-Muñoz, O. M.; Banqueri, J.; Fernández-Ramos, M. D.; Capitán-Vallvey, L. F. *Anal. Chim. Acta* **2009**, *655*, 66–74.
- (27) Capitán-Vallvey, L. F.; Palma, A. J. *Anal. Chim. Acta* **2011**, *696*, 27–46.
- (28) Schäferling, M.; Wu, M.; Enderlein, J.; Bauer, H.; Wolfbeis, O. S. *Appl. Spectrosc.* **2003**, *57*, 1386–1392.
- (29) Park, J.; Hong, W.; Kim, C. S. *IEEE Sens. J.* **2010**, *10*, 1855–1862.
- (30) Bansal, A. K.; Holzer, W.; Penzkofer, A.; Tsuboi, T. *Chem. Phys.* **2006**, *330*, 118–129.
- (31) Eaton, K.; Douglas, B.; Douglas, P. *Sens. Actuators, B: Chem.* **2004**, *97*, 2–12.
- (32) Capitán-Vallvey, L. F.; Asensio, L. J.; López-González, J.; Fernández-Ramos, M. D.; Palma, A. J. *Anal. Chim. Acta* **2007**, *583*, 166–173.
- (33) Wang, X.; Meier, R. J.; Link, M.; Wolfbeis, O. S. *Angew. Chem., Int. Ed.* **2010**, *49*, 4907–4909.
- (34) Mayr, T.; Abel, T.; Enko, B.; Borisov, S.; Konrad, C.; Köstler, S.; Lamprecht, B.; Sax, S.; List, E. J. W.; Klimanta, I. *Analyst* **2009**, *134*, 1544–1547.
- (35) Courbat, J.; Briand, D.; Wöllenstein, J.; de Rooij, N. F. *Sens. Actuators, B: Chem.* **2011**, *160*, 910–915.
- (36) Saini, D. P.; Klainer, S. M.; Coulter, S. L. *Chip level waveguide sensor*. U.S. Patent 5,737,457, April 7, 1998.
- (37) Finkenzeller, K. *RFID Handbook*, 2nd ed.; Wiley: New York, 2003.
- (38) Rida, A.; Yang, L.; Vyas, R.; Tentzeris, M. M. *IEEE Antennas Propag. Mag.* **2009**, *51*, 13–23.
- (39) Vyas, R.; Lakafosis, V.; Rida, A.; Chaisilwattana, N.; Travis, S.; Pan, J.; Tentzeris, M. M. *IEEE Trans. Microwave Theory Tech.* **2009**, *57*, 1370–1382.
- (40) Mohan, S. S.; Hershenson, M. D. M.; Boyd, S. P.; Lee, T. H. *IEEE J. Solid-State Circuit.* **1999**, *34*, 1419–1420.
- (41) Salmerón, J. F.; Capitán-Vallvey, L. F. M.; Palma, A. J.; Molina-Lopez, F.; Briand, D.; de Rooij, N. F. Physical and Electrical Properties of Ink-jet and Screen Printed Patterns for RFID HF Antennas. *IEEE International Conference on RFID-Technologies and Applications (RFID-TA)*, Nice, France, 2012; pp 188–192.
- (42) Pérez de Vargas-Sansalvador, I. M.; Martínez-Olmos, A.; Palma, A. J.; Fernández-Ramos, M. D.; Capitán-Vallvey, L. F. *Microchim. Acta.* **2011**, *172*, 455–464.
- (43) Carraway, E. R.; Demas, J. N.; De Graff, B. A.; Bacon, J. R. *Anal. Chem.* **1991**, *63*, 337–342.